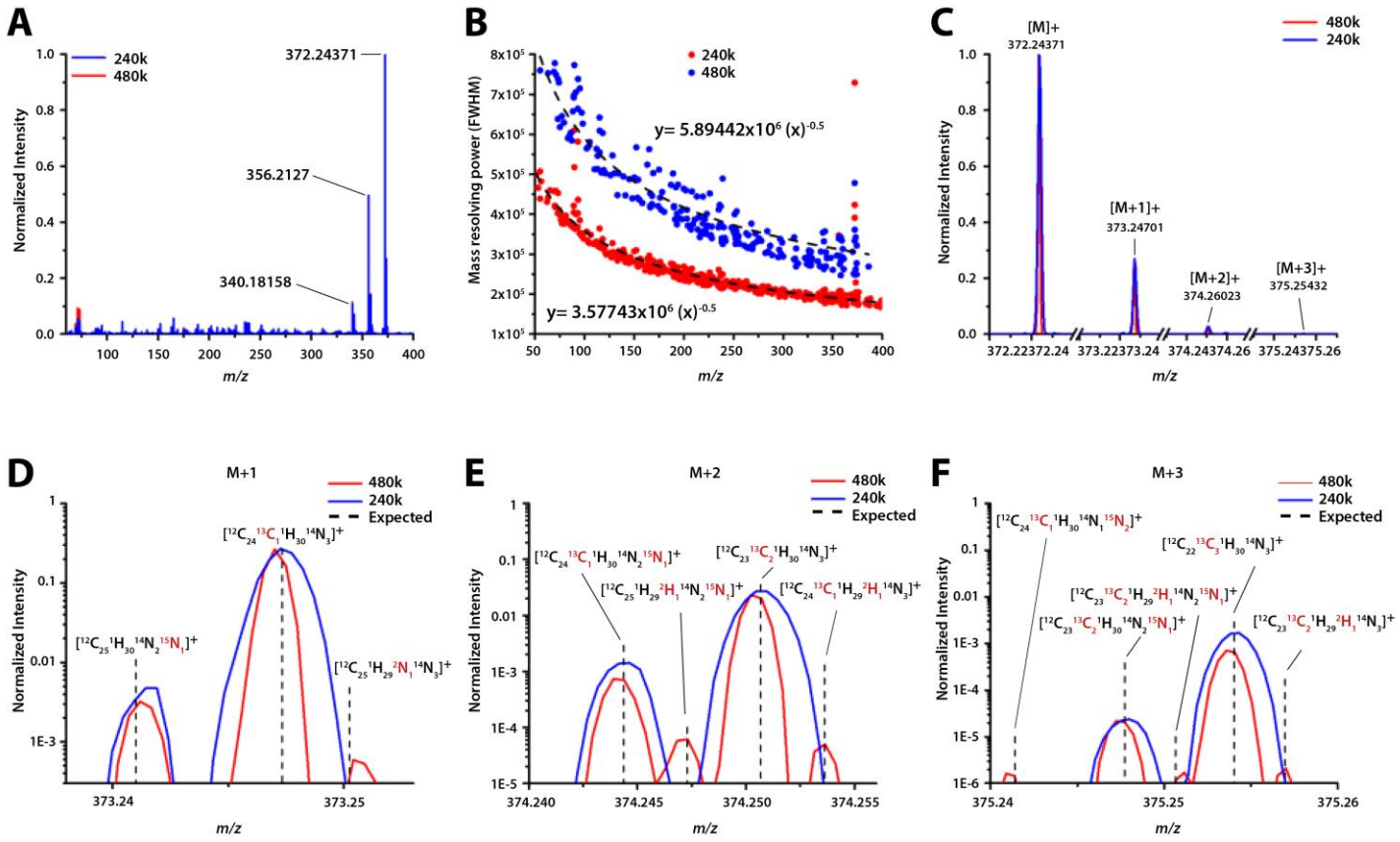

Supplementary Figure 1

Resolving crystal violet isotope fine structure with high mass resolving power of the Orbitrap.

A) Positive ion mass spectra of crystal violet ($[C_{25}H_{30}N_3]^+$ at *m/z* 372.24371) at nominal resolution settings 240,000 (blue) and 480,000 (red) mass resolving power (mode 2) normalized to the molecular ion peak. B) Mass resolving power for secondary ions in the mass spectrum with fits of the expected $m^{-0.5}$ relationship. At *m/z* 200 the mass resolving power is approximately 253,000 (0.5 s transient) and 417,000 (1 s transients). C) The isotopic distribution of the crystal violet molecular ion. D-F) Annotated spectra for the M+1, M+2 and M+3 isotope peaks for crystal violet spanning a dynamic range of five orders of magnitude (100% abundance to 0.001 % abundance). Results presented are from a single measurement.

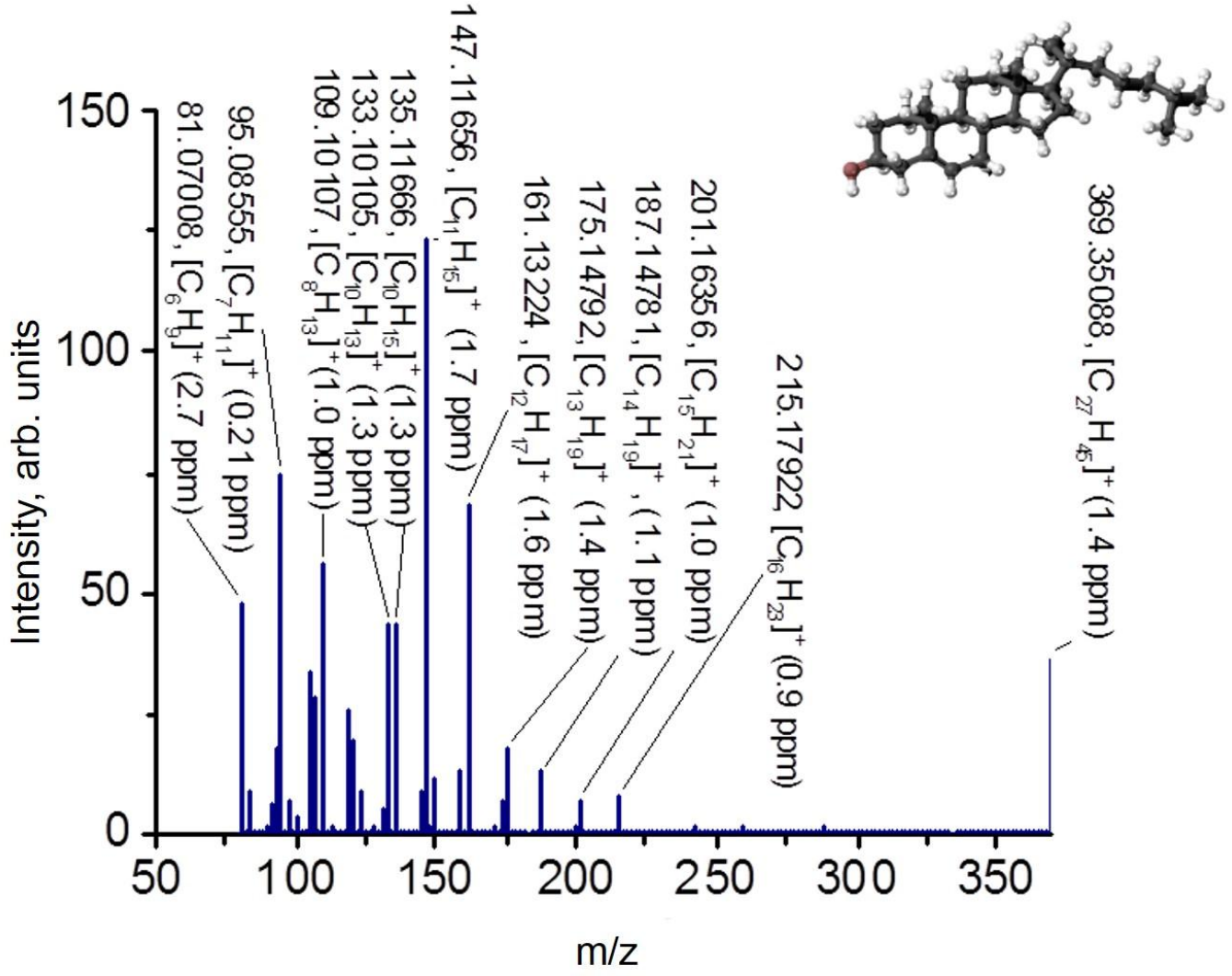

Supplementary Figure 2

In situ tandem MS of cholesterol.

Orbitrap tandem MS of cholesterol fragment $[M\text{-}H_2O+H]^+$ from the corpus callosum of a mouse brain section. Peaks are annotated with chemical formulae and mass deviation. The fragment ion peaks were identified by their accurate mass. Result presented is from a single measurement.

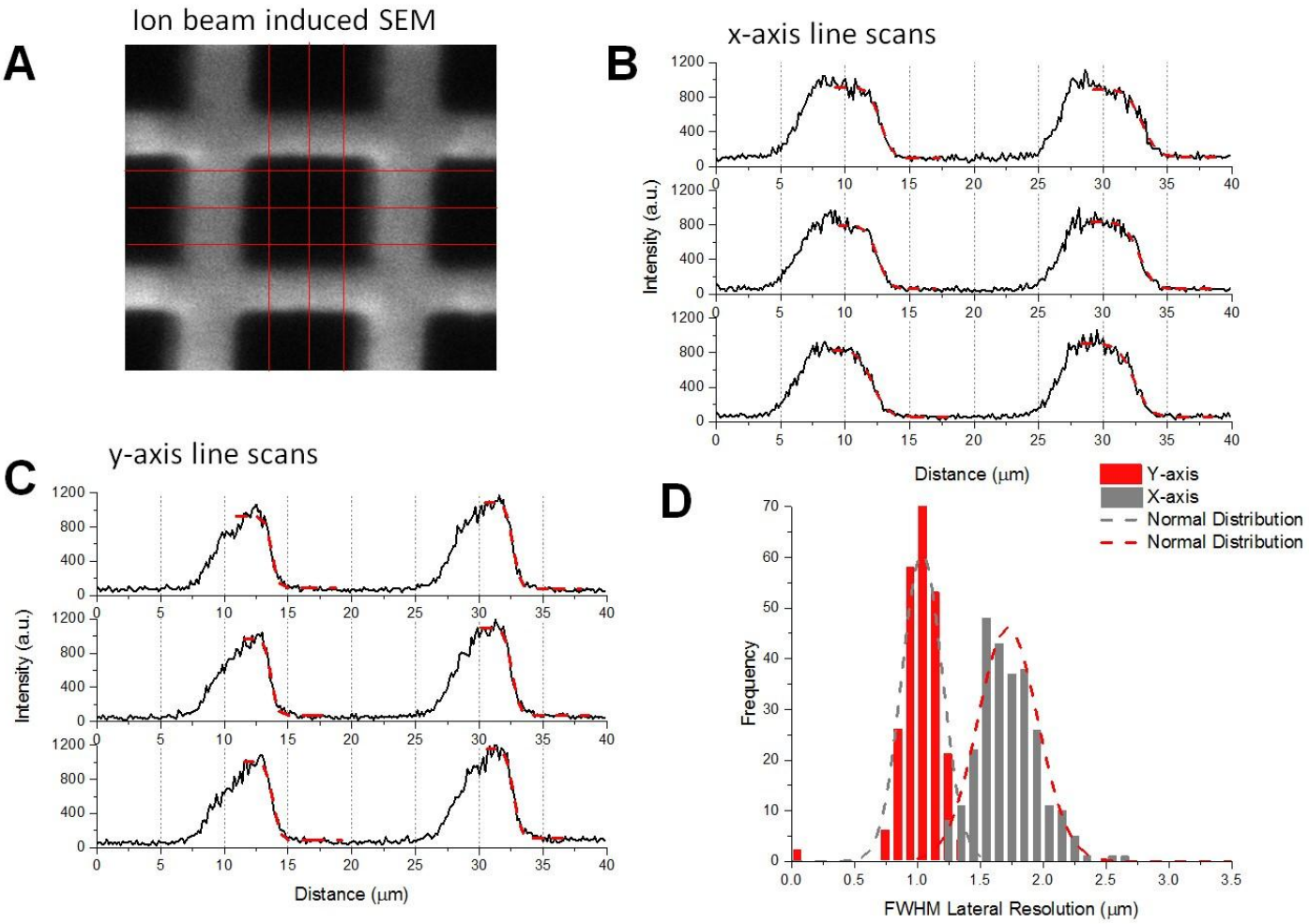

Supplementary Figure 3

Lateral resolution measurement for the focused GCIB primary ion beam (with the secondary ion extraction potential off).

A) Ion induced secondary electron image of an electroformed mesh grid over a hole obtained with the Ar_{3000}^{+} primary ion beam. Red lines along the *x* and *y* axes denote the location of linescans used to measure the resolution. B and C) Representative line scans of the secondary electron intensity across the edge of the grid for the *x*-axis and *y*-axis, respectively. D) The distribution of the FWHM lateral resolution measurements with a fit to a normal distribution function (dotted line, bin size 0.1 μm). The average FWHM lateral resolution was 1.72 μm ± 0.24 μm (μ ± 1σ) (*n*=246, grey bars) across the *x*-axis and 1.04 μm ± 0.16 μm (μ ± 1σ) (*n*=246, red bars) across the *y*-axis. Results presented are from a single image.

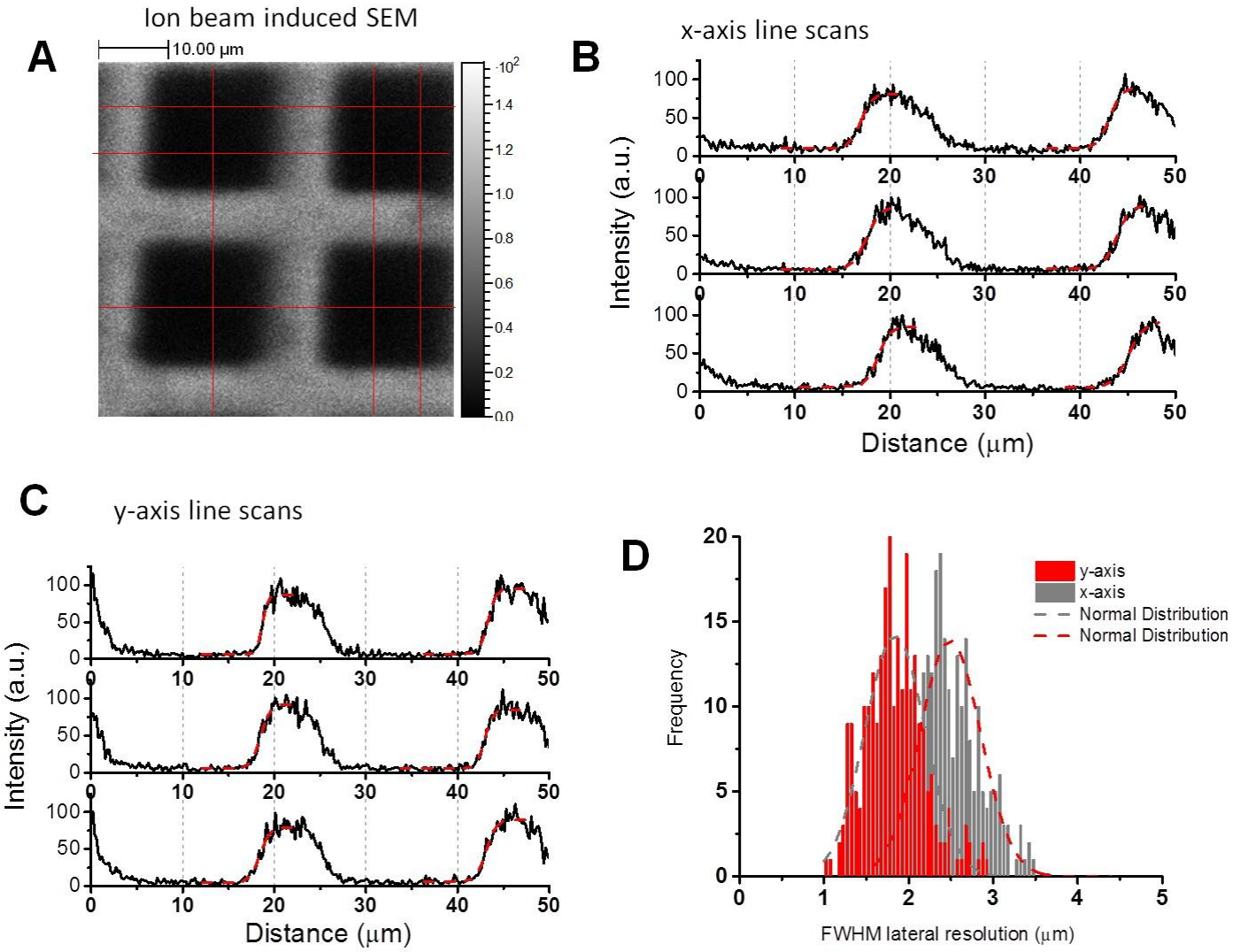

Supplementary Figure 4

Lateral resolution measurement for the focused GCIB primary ion beam (with the secondary ion extraction potential on, as in all SIMS analyses).

A) Ion induced secondary electron image of an electroformed mesh grid over a hole obtained with the Ar_{3000}^{+} primary ion beam. Red lines along the *x* and *y* axes denote the location of linescans used to measure the resolution. B and C) Representative line scans of the secondary electron intensity across the edge of the grid for the *x*-axis and *y*-axis, respectively. D) The distribution of the FWHM lateral resolution measurements with a fit to a normal distribution function (dotted line, bin size 0.05 µm). The average FWHM lateral resolution was 2.49 µm ± 0.36 µm (µ ± 1σ) (*n*=243, grey bars) across the *x*-axis and 1.84 µm ± 0.36 µm (µ ± 1σ) (*n*=254, red bars) across the *y*-axis. Results presented are from a single image.

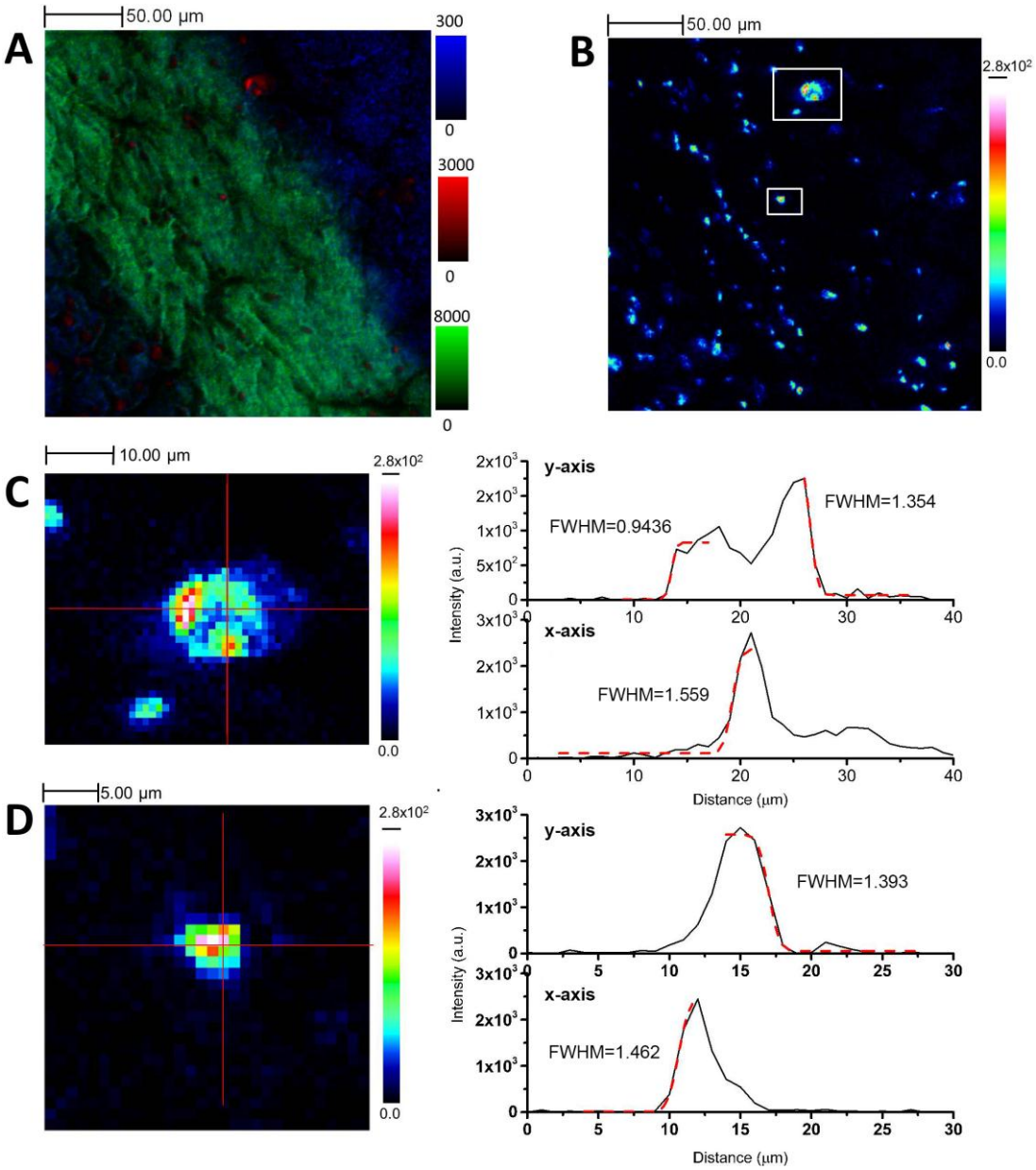

Supplementary Figure 5

Lateral resolution measurement for the focused 20 keV Ar_{3000}^{+} GCIB primary ion beam for biomolecules.

A) Overlay ion image of selected sulfatide peaks (green), phosphatidylinositol peaks (blue) and nuclear markers (red). [Sulfatide peaks: C22(OH) ($[C_{46}H_{88}NO_{12}SO]^-$ at *m/z* 878.6035, (0.3 ppm)), C24:1 ($[C_{48}H_{90}NO_{11}S]^-$ at *m/z* 888.6242 (0.3 ppm)) and C24:1(OH) ($[C_{48}H_{90}NO_{12}S]^-$ at m/z 904.6192 (0.3 ppm)); PI peaks: PI(38:4) ($[C_{47}H_{82}O_{13}P]^-$ at *m/z* 885.5502 (0.3 ppm)) and PI head-group ($[C_6H_{10}PO_8]^-$ at *m/z* 241.0120 (0.6ppm)); Nuclear markers $[C_4N_3]^-$ at *m/z* 90.0095 (2.8 ppm), $[CN_2O_2P]^-$ at *m/z* 102.9702 (0.6 ppm), $[C_4H_2N_4]^-$ at *m/z* 106.0285 (0.3 ppm), $[C_4H_3N_4]^-$ at *m/z* 107.0207 (0.2 ppm), $[C_5HN_4]^-$ at *m/z* 117.0207 (0.2 ppm), $[C_5H_3N_4]^-$ at *m/z* 119.0363 (0.3 ppm), $[C_5HN_4O]^-$ at *m/z* 133.0156 (0.1 ppm) and $[C_5H_4N_5]^-$ at *m/z* 134.0472 (6 ppb). B) Polychromatic ion image of the nuclear markers with regions of interest outlined in white. C) Detail of one nucleus from B) with line scans across the x-axis and y-axis. D) as C) for the second nucleus. Average resolution determined to be 1.34 µm ± 0.24 µm (*n*=5).

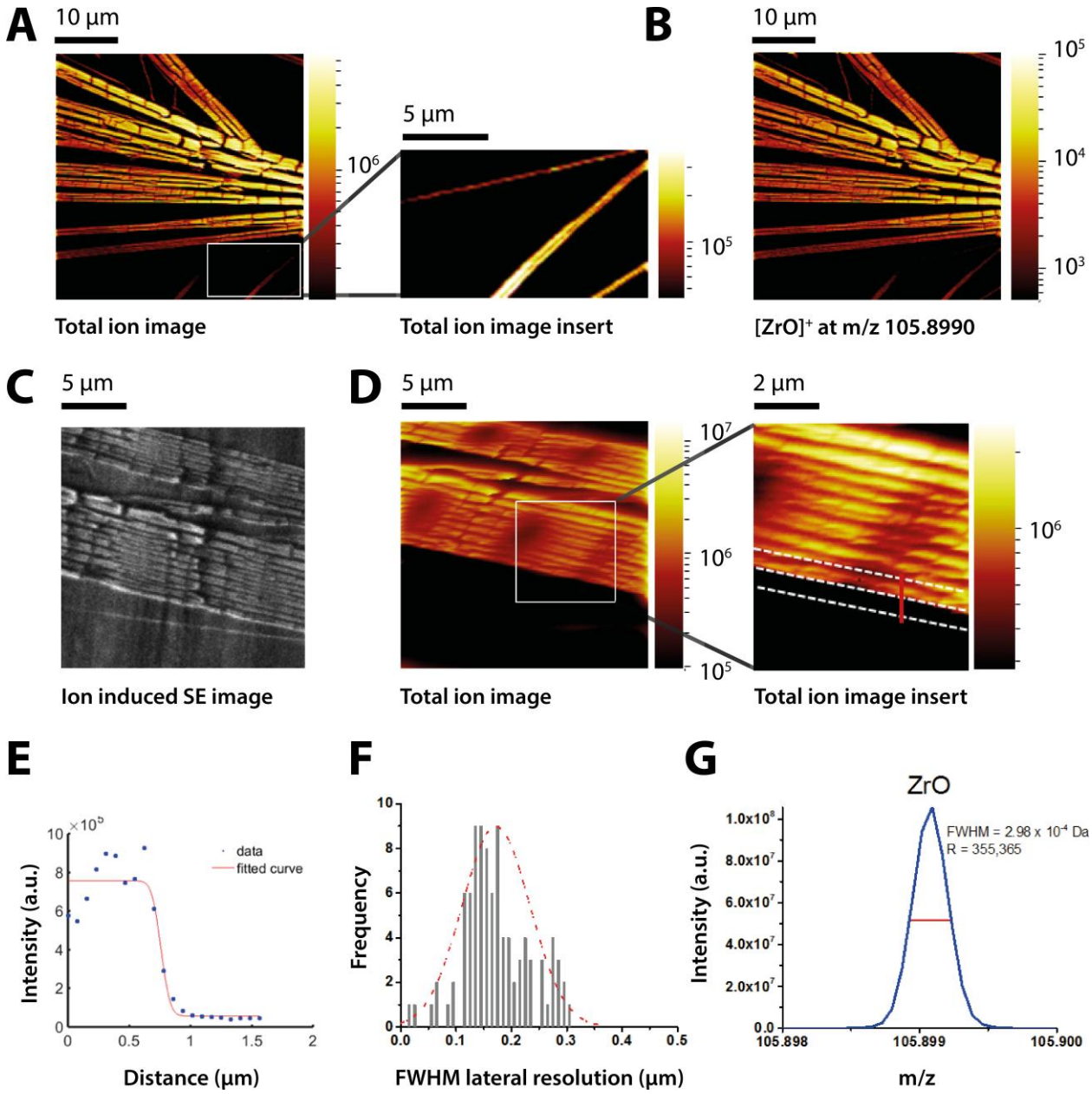

Supplementary Figure 6

Measurement of the Bi LMIG simultaneous lateral resolution and mass resolving power.

(A) Total ion images of ZrO_2 crystals (mode 7) obtained with the Bi LMIG source with insert showing detail of thin nanostructures. B) Ion image of the $[ZrO]^+$ peak at *m/z* 105.8990 (0.5 ppm). C) Ion induced SE image of the ZrO_2 crystal before analysis. D) Total ion images of ZrO_2 crystals (mode 7) obtained with the Bi LMIG source and insert region of interest for resolution measurement outlined in white. Linescans were obtained along the *y*-axis of the ion image across the ZrO_2 crystal edge. E) A representative line scan shows the total ion intensity across the ZrO_2 interface.. F) The distribution of lateral resolution measurements with a fit a normal distribution function (red dotted line, bin size 0.01 µm). The average FWHM lateral resolution was 172 nm ± 61 nm (µ ± 1σ) (*n*=95). G) The $[ZrO]^+$ peak at m/z 105.8991 (0.2 ppm) with a FWHM width of 0.3 mDa and mass resolving power of 355,000. Results presented are from a single image.

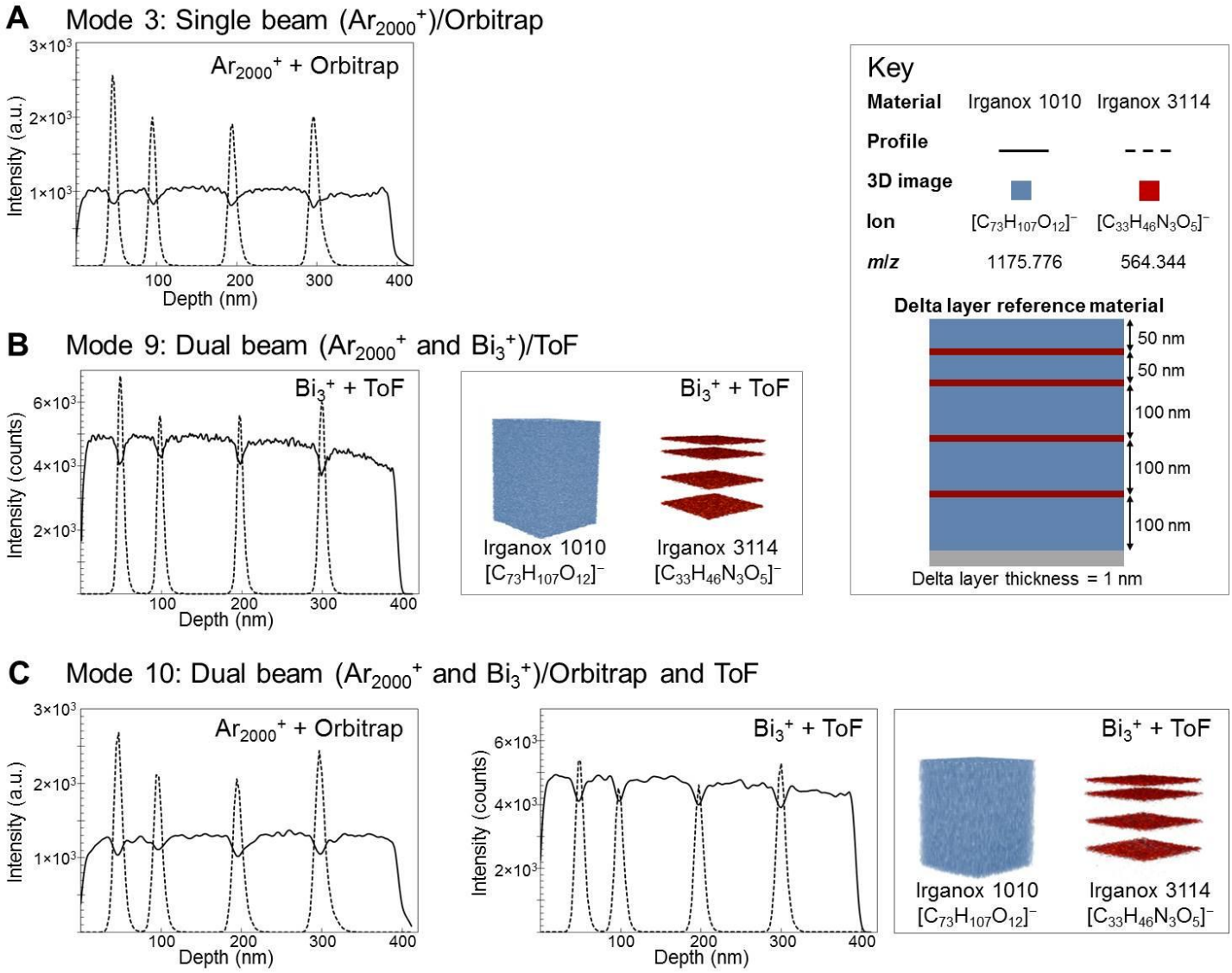

Supplementary Figure 7

3D imaging of an Irganox delta layer reference material.

A) Orbitrap MS (mode 3), 5 keV Ar_{2000}^+ sputtering and analysis, intensity depth profile of the Irganox 1010 molecular ion, $[C_{73}H_{107}O_{12}]^-$ at *m/z* 1175.776 (solid line), and fragment ion from Irganox 3114, $[C_{33}H_{46}N_3O_5]^-$ at *m/z* 564.344 (dashed line). B) ToF MS (mode 9), 5 keV Ar_{2000}^+ sputtering and 30 keV Bi_3^+ analysis intensity depth profile, as A) with 3D reconstruction from ToF MS data and C) Dual analyser, dual beam mode (10) with 5 keV Ar_{2000}^+ sputter beam. Intensity depth profiles as A) for Orbitrap MS Ar_{2000}^+ analysis beam and ToF MS 30 keV Bi_3^+ beam, with 3D reconstruction from ToF MS data. Results presented are from a single measurement.

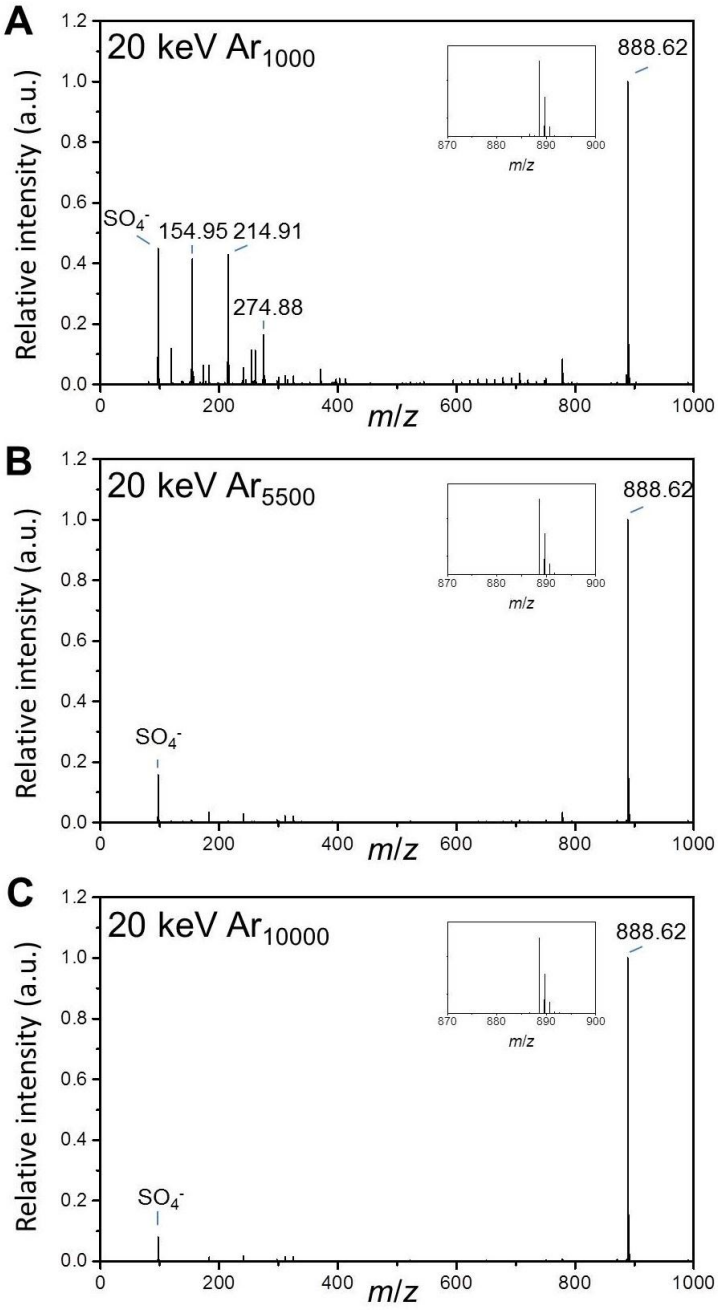

Supplementary Figure 8

20 keV Ar_n GCIB Orbitrap negative ion MS of reference lipid C24:1 Mono-Sulfo Galactosyl(ß) Ceramide (d18:1/24:1) ($C_{48}H_{90}NO_{11}S$).

(A) n = 1000, (B) n = 5500 and (C) n = 10000. Inset shows detail of the molecular ion, $C_{48}H_{90}NO_{11}S^-$, revealing little fragmentation for this particular species. Results presented are from single measurements.

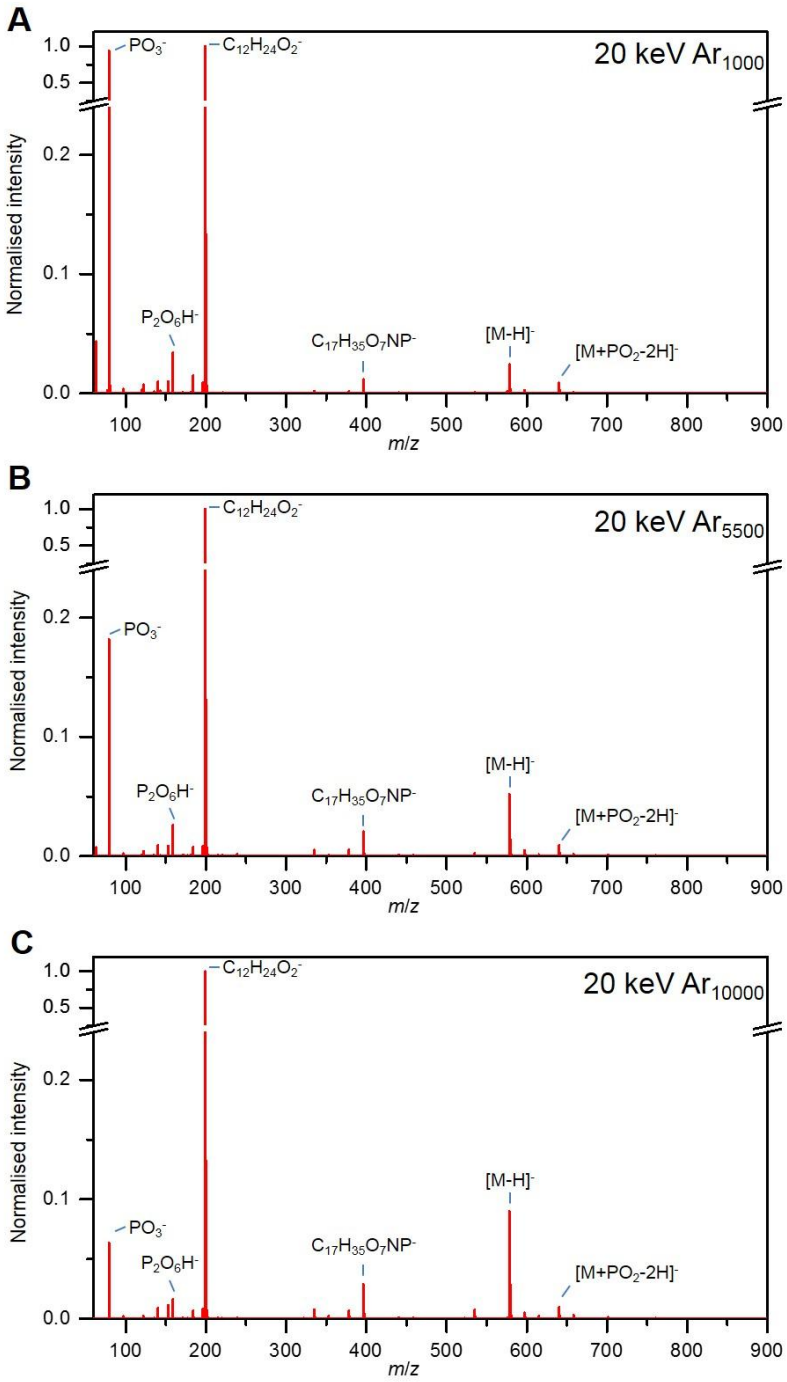

Supplementary Figure 9

20 keV Ar_n GCIB Orbitrap positive ion MS of reference lipid 1,2-dilauroyl-sn-glycero-3-phosphoethanolamine ($C_{29}H_{58}NO_8P$), normalised to the $C_{12}H_{22}O_2^-$ peak intensity.

(A) *n* = 1000, (B) *n* = 5500 and (C) *n* = 10000. Results presented are from single measurements.

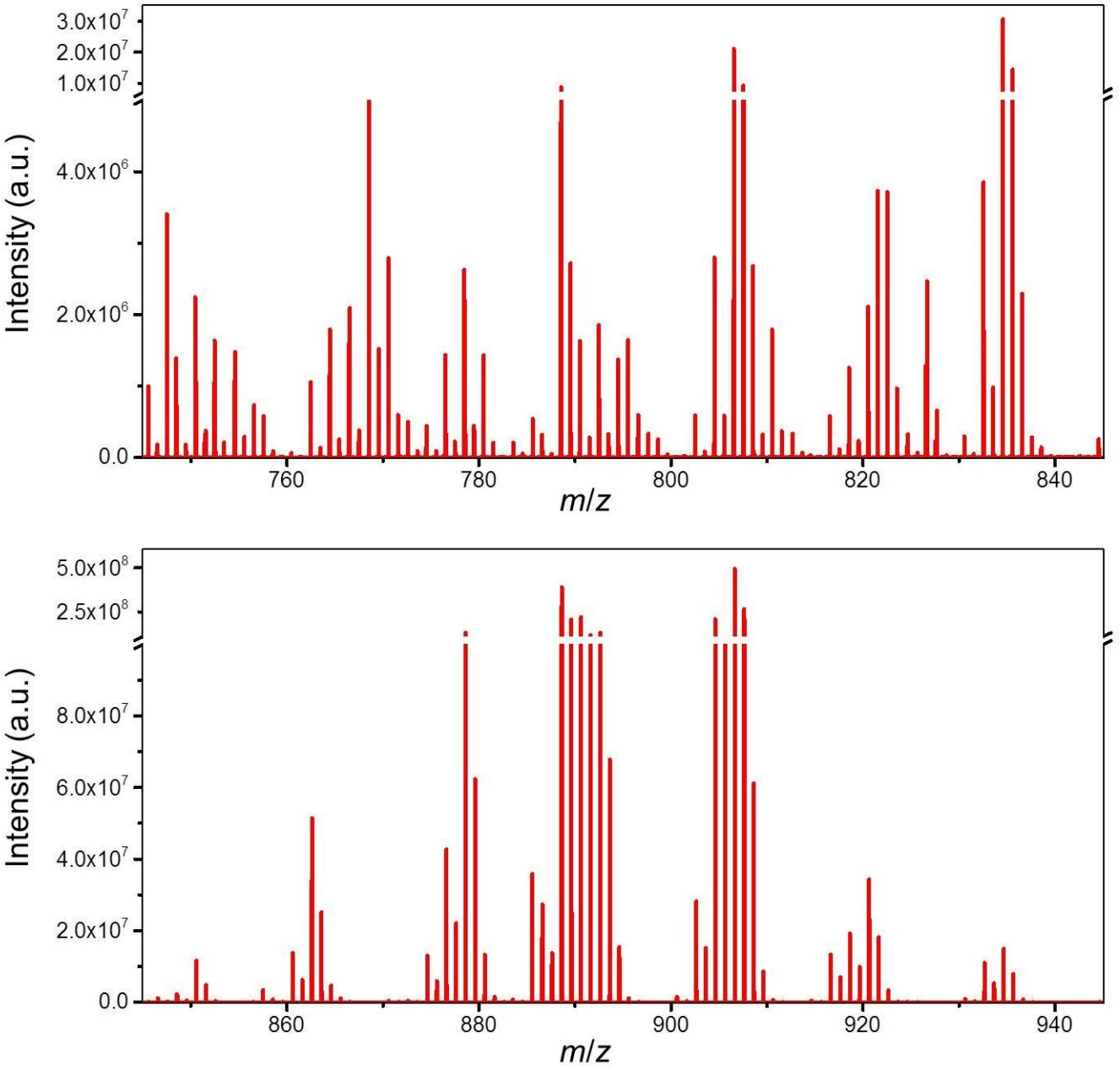

Supplementary Figure 10

Lipid region from the negative ion image from Figure 3D in the main text (mode 7).

The spectra was summed over the entire ion image. See Supplementary Tables 2 and 3 for annotations. Result presented is from a single measurement.

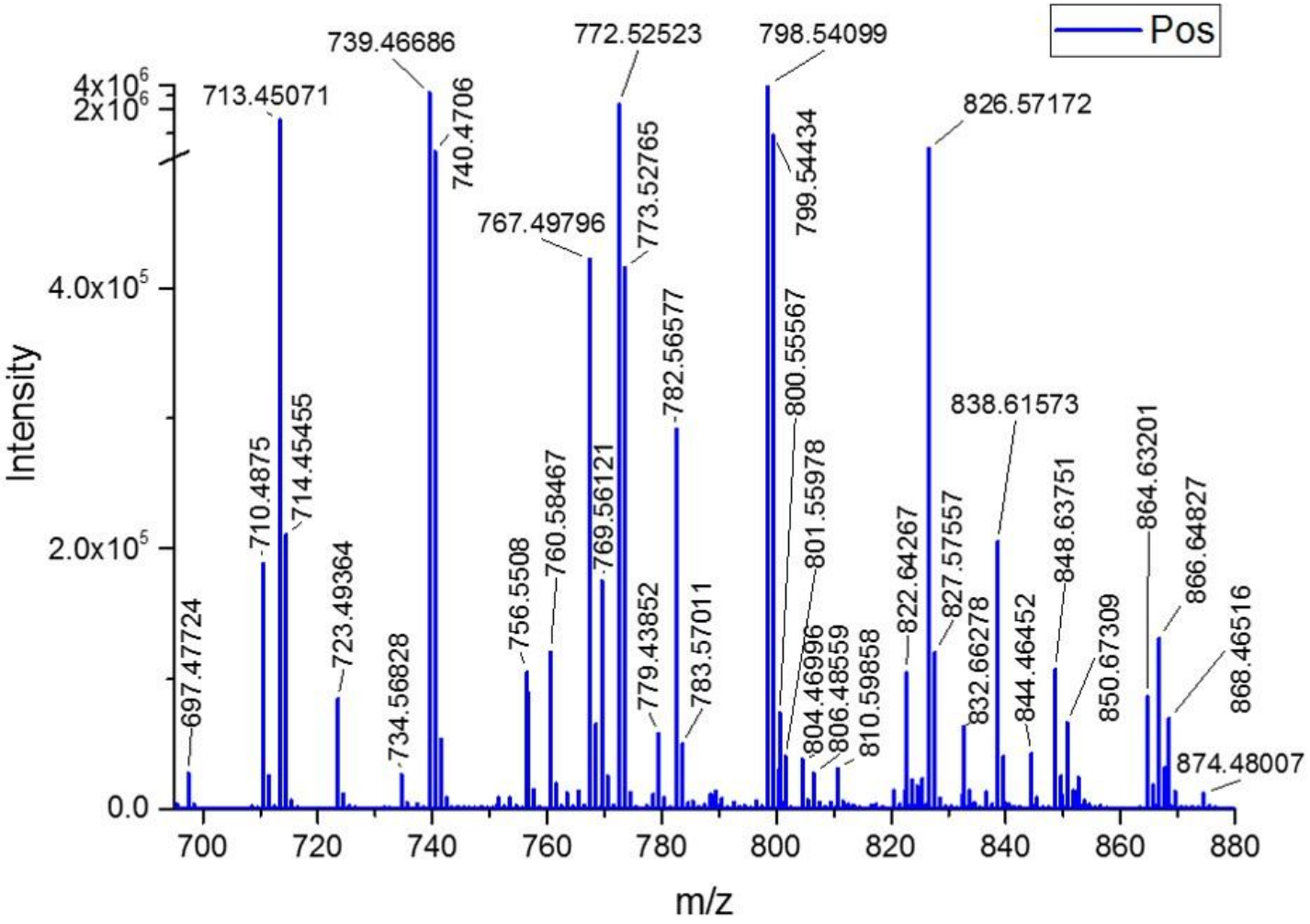

Supplementary Figure 11

Positive ion Orbitrap MS obtained from the CA3 vicinity of the hippocampus on a coronal brain section.

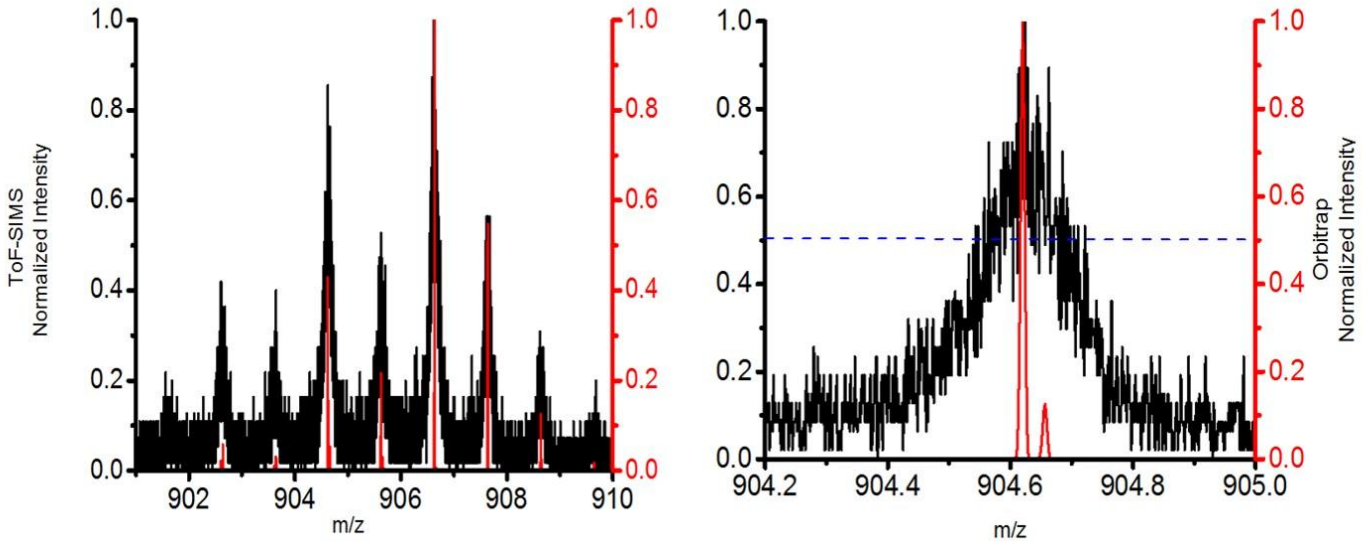

Supplementary Figure 12

Comparison of resolving power of ToF MS (mode 1) and Orbitrap MS (mode 2) for intact lipids from mouse hippocampus.

(A) Negative ion mass spectra between *m/z* 902 – *m/z* 910 (red = Orbitrap MS (mode 2), black = ToF MS (mode 1)). B) Detail of spectra between *m/z* 904.2 – *m/z* 905.0. Result presented is from a single measurement.

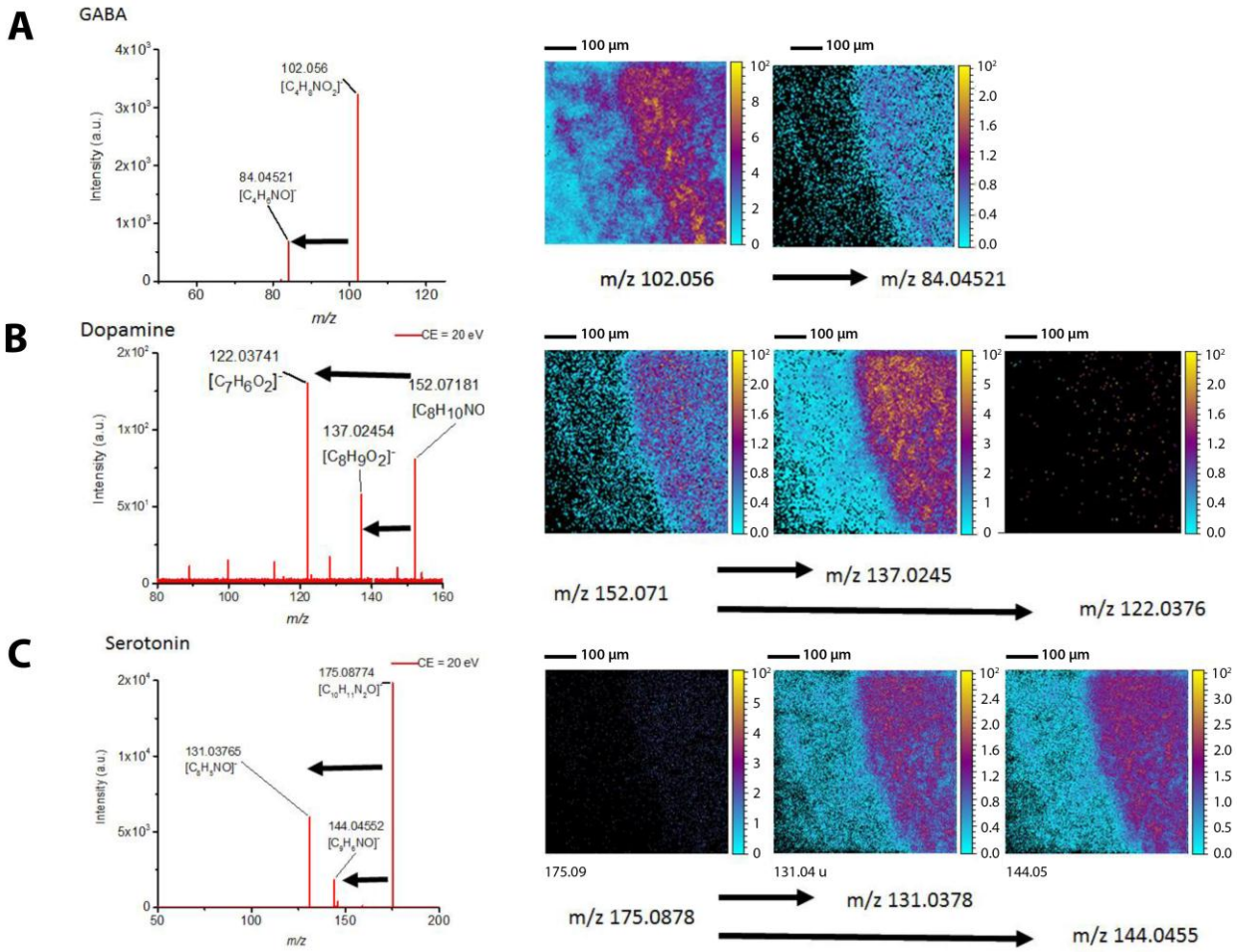

Supplementary Figure 13

20 keV Ar_{3000}^{+} GCIB Orbitrap negative ion MS/MS of reference neurotransmitters using 20 eV collision energy.

(A) GABA $[M-H]^-$, (B) dopamine $[M-H]^-$ and (C) serotonin $[M-H]^-$. Inset images show the co-localised spatial distribution of these secondary ions from the data in Figure 5. Results presented are from single measurements.

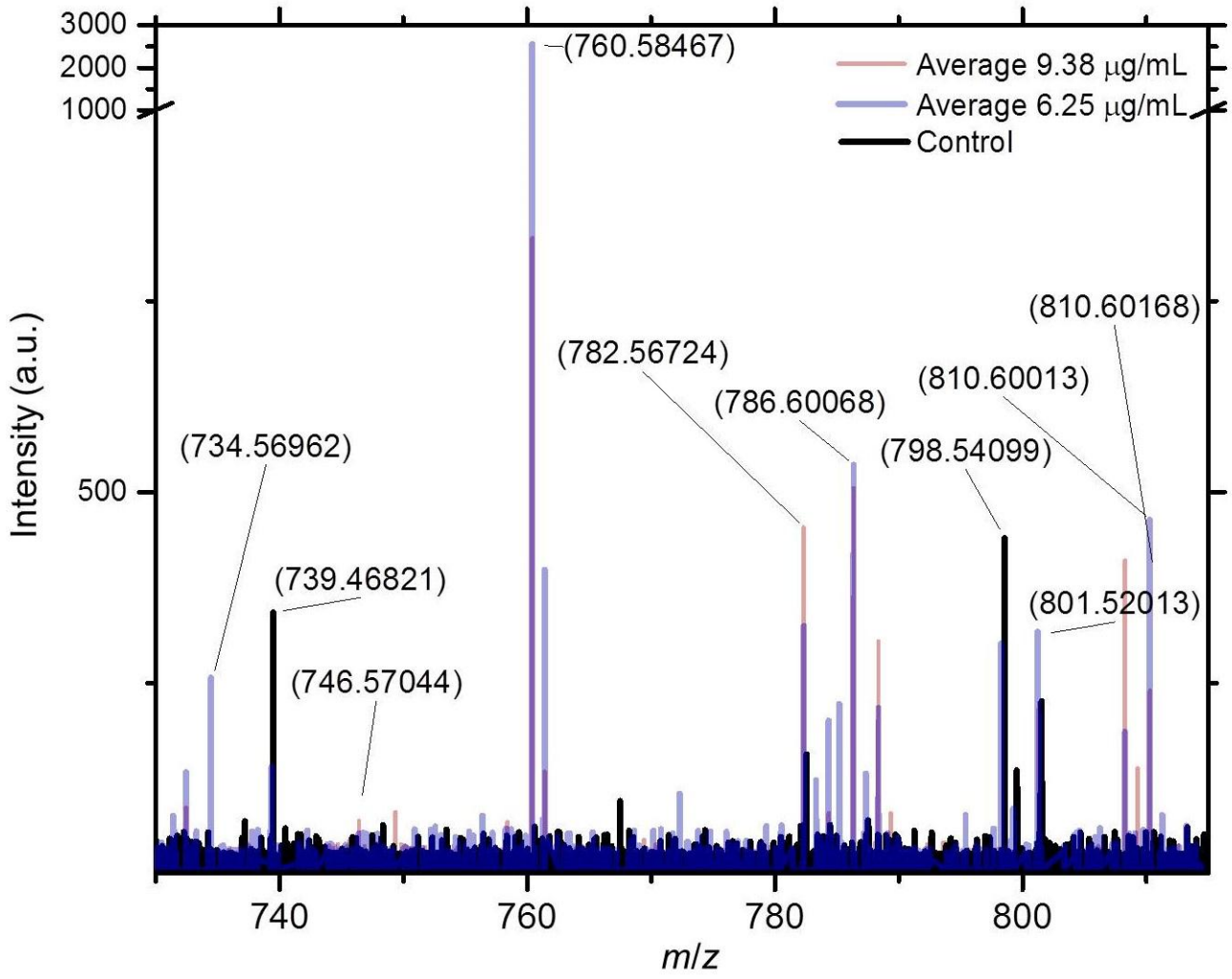

Supplementary Figure 14

Orbitrap MS of lipids in control and amiodarone treated macrophage cells.

The average positive ion mass spectra for control cells (*n*=8) and treated cells (6.25 μg/ml (*n*=3) and 9.38 μg/ml (*n*=7)).

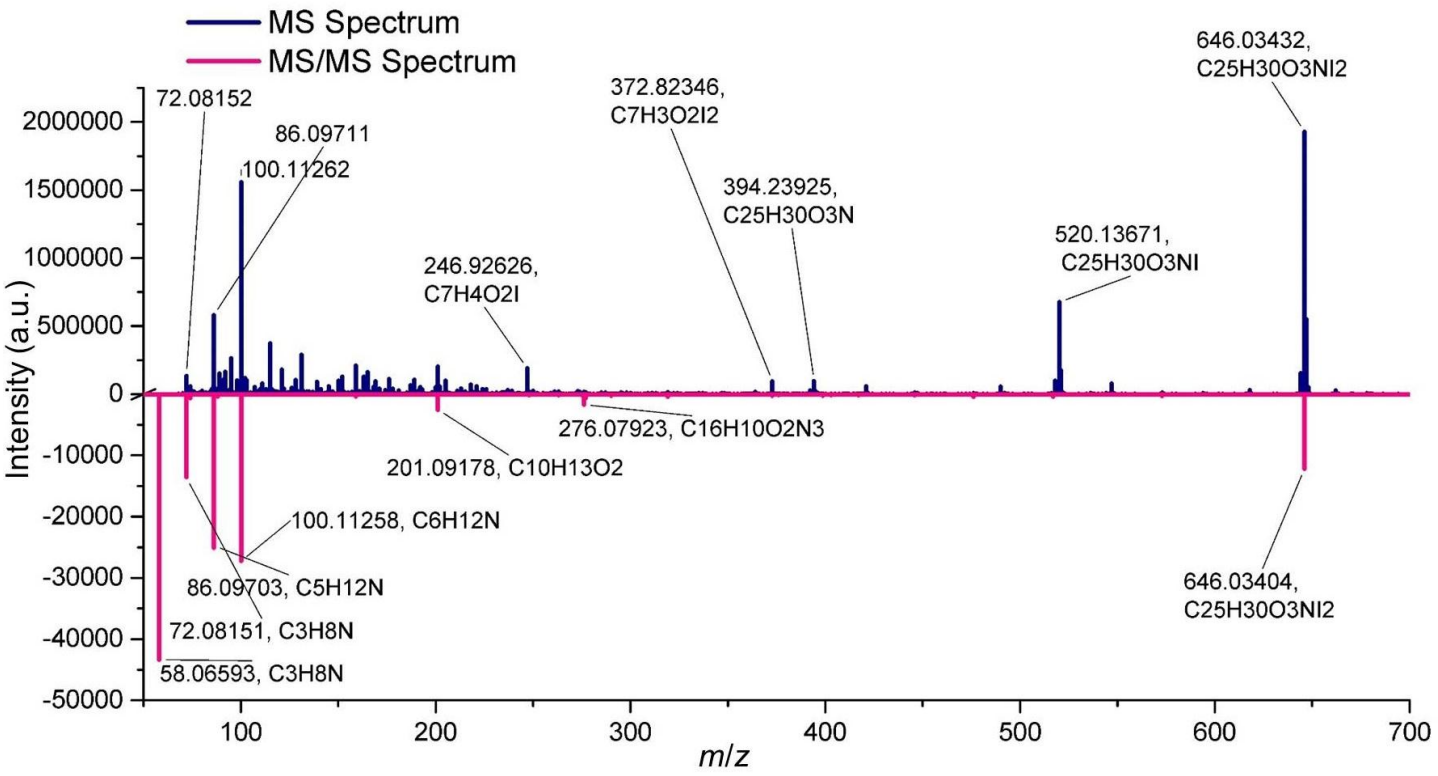

Supplementary Figure 15

Full MS and tandem MS spectra of reference sample of amiodarone.

20 keV Ar_{3000}^{+} Orbitrap MS (mode 2) spectrum (blue, positive intensity scale) and tandem MS of the $[M+H]^{+}$ peak (red, negative intensity scale). Results presented are from single measurements.

The 3D OrbiSIMS – Label-Free Metabolic Imaging with Sub-cellular Lateral Resolution and High Mass Resolving Power

Melissa K Passarelli, Alexander Pirkl, Rudolf Moellers, Dmitry Grinfeld, Felix Kollmer, Rasmus Havelund, Carla F. Newman, Peter S. Marshall, Henrik Arlinghaus, Morgan R. Alexander, Andy West, Stevan Horning, Ewald Niehuis, Alexander Makarov, Colin T. Dollery and Ian S. Gilmore*

Supplementary Table 1. Summary of the crystal violet isotope peaks in the 3D OrbiSIMS (mode 2) spectrum using 0.5 s (240 k mass resolving power) and 1 s (480 k mass resolving power) transients.

Isotope	*m/z*	Relative abundance (%)	Chemical formula	Resolved @240 k	Resolved @480 k
M	372.24397	100.000	$[^{12}C_{25}{}^{1}H_{30}{}^{14}N_3]+$	Y	Y
M+1	373.24101	1.084	$[^{12}C_{25}{}^{1}H_{30}{}^{14}N_2{}^{15}N_1]+$	Y	Y
	373.24733	27.039	$[^{12}C_{24}{}^{13}C_1{}^{1}H_{30}{}^{14}N_3]+$	Y	Y
	373.25025	0.480	$[^{12}C_{25}{}^{1}H_{29}{}^{2}H_1{}^{14}N_3]+$	Y	Y
M+2	374.23804	0.004	$[^{12}C_{25}{}^{1}H_{30}{}^{14}N_1{}^{15}N_2]+$	N	Y
	374.24437	0.293	$[^{12}C_{24}{}^{13}C_1{}^{1}H_{30}{}^{14}N_2{}^{15}N_1]+$	Y	Y
	374.24729	0.005	$[^{12}C_{25}{}^{1}H_{29}{}^{2}H_1{}^{14}N_2{}^{15}N_1]+$	Y	Y
	374.25068	3.509	$[^{12}C_{23}{}^{13}C_2{}^{1}H_{30}{}^{14}N_3]+$	Y	Y
	374.25361	0.130	$[^{12}C_{24}{}^{13}C_1{}^{1}H_{29}{}^{2}H_1{}^{14}N_2]+$	Y	Y
	374.25652	0.001	$[^{12}C_{25}{}^{1}H_{28}{}^{2}H_2{}^{14}N_3]+$	N	Y
M+3	375.2414	0.001	$[^{12}C_{24}{}^{13}C_1{}^{1}H_{30}{}^{14}N_1{}^{15}N_2]+$	N	Y
	375.24772	0.038	$[^{12}C_{23}{}^{13}C_2{}^{1}H_{30}{}^{14}N_2{}^{15}N_1]+$	Y	Y
	375.25065	0.001	$[^{12}C_{24}{}^{13}C_1{}^{1}H_{29}{}^{2}H_1{}^{14}N_2{}^{15}N_1]+$	N	Y
	375.25404	0.291	$[^{12}C_{22}{}^{13}C_3{}^{1}H_{30}{}^{14}N_3]+$	Y	Y
	375.25696	0.017	$[^{12}C_{23}{}^{13}C_2{}^{1}H_{29}{}^{2}H_1{}^{14}N_3]+$	Y	Y
M+4	376.25108	0.003	$[^{12}C_{22}{}^{13}C_3{}^{1}H_{30}{}^{14}N_2{}^{15}N_1]+$	N	Y

Nature Methods: doi:10.1038/nmeth.4504

Supplementary Table 2. Putative annotation of (3'-sulfo)Galβ-N-(acyl)-sphing-4-enine species detected in the negative ion image of the mouse hippocampus in Figure 3D (main text).

Lipid	Chemical formula of $[M-H]^-$ ion	Mass (Da)	Intensity (a.u.)	Mass accuracy (ppm)
Sulfatides Note: All sulfatides could potentially have d18:0 or d18:2 moieties, instead of the normally dominating d18:1.				
C14 Sulfatide	$[C_{38}H_{72}NO_{11}S]^-$	750.4832	5.84×10^4	0.5
C14:1 (OH) Sulfatide	$[C_{38}H_{70}NO_{12}S]^-$	764.4624	6.50×10^4	0.5
C14 (OH) Sulfatide	$[C_{38}H_{72}NO_{12}S]^-$	766.4781	4.67×10^4	0.3
C16:1 Sulfatide	$[C_{40}H_{74}NO_{11}S]^-$	776.4988	1.13×10^5	0.4
C16 Sulfatide	$[C_{40}H_{76}NO_{11}S]^-$	778.5145	1.04×10^5	0.4
C16:1(OH) Sulfatide	$[C_{40}H_{74}NO_{12}S]^-$	792.4937	5.85×10^4	0.4
C16 (OH) Sulfatide	$[C_{40}H_{76}NO_{12}S]^-$	794.5094	3.80×10^4	0.4
C18:1 Sulfatide	$[C_{42}H_{78}NO_{11}S]^-$	804.5301	3.72×10^5	0.3
C18 Sulfatide	$[C_{42}H_{80}NO_{11}S]^-$	806.5458	1.94×10^7	0.3
C18:1 (OH) Sulfatide	$[C_{42}H_{78}NO_{12}S]^-$	820.5250	1.41×10^5	0.2
C18 (OH) Sulfatide	$[C_{42}H_{80}NO_{12}S]$-	822.5407	1.03×10^7	0.2
C20:1 Sulfatide	$[C_{44}H_{82}NO_{11}S]$-	832.561	1.62×10^5	0.3
C20 Sulfatide	$[C_{44}H_{84}NO_{11}S]$-	834.5771	1.13×10^6	0.3
C20:1(OH) Sulfatide	$[C_{44}H_{82}NO_{12}S]$-	848.5563	1.47×10^5	0.7
C20(OH) Sulfatide	$[C_{44}H_{84}NO_{12}S]$-	850.5720	5.59×10^6	0.7
C22:2 Sulfatide	$[C_{46}H_{84}NO_{11}S]$-	858.5771	8.66×10^4	0.7
C22:1 Sulfatide	$[C_{46}H_{86}NO_{11}S]^-$	860.5927	7.37×10^6	0.6
C22 Sulfatide	$[C_{46}H_{88}NO_{11}S]^-$	862.6084	1.97×10^7	0.7
C22:1(OH) Sulfatide	$[C_{46}H_{86}NO_{12}S]^-$	876.5876	6.05×10^6	0.6
C22 (OH) Sulfatide	$[C_{46}H_{88}NO_{12}S]^-$	878.6033	6.86×10^7	0.6
C24:2 Sulfatide	$[C_{48}H_{88}NO_{11}S]^-$	886.6084	1.14×10^7	0.5
C24:1 Sulfatide	$[C_{48}H_{90}NO_{11}S]^-$	888.6240	1.81×10^8	0.5
C24 Sulfatide	$[C_{48}H_{92}NO_{11}S]^-$	890.6397	3.93×10^7	1.5
C24:1(OH) Sulfatide	$[C_{48}H_{90}NO_{12}S]^-$	904.6189	4.91×10^7	0.5
C24 (OH) Sulfatide	$[C_{48}H_{92}NO_{12}S]^-$	906.6346	6.16×10^7	0.6
C26:1 Sulfatide	$[C_{50}H_{94}NO_{11}S]^-$	916.6553	1.33×10^5	0.3
C26 Sulfatide	$[C_{50}H_{96}NO_{11}S]$-	918.6710	1.21×10^4	-0.9
C26:1 (OH) Sulfatide	$[C_{50}H_{94}NO_{12}S]^-$	932.6502	9.79×10^4	0.3
C26 (OH) Sulfatide	$[C_{50}H_{96}NO_{12}S]^-$	934.6659	3.41×10^4	0.4

Nature Methods: doi:10.1038/nmeth.4504

Supplementary Table 3. Putative annotation of Glycerophospholipids species detected in the negative ion image of the mouse hippocampus in Figure 3D (main text).

Lipid	Chemical formula of $[M-H]^-$ ion	Mass (Da)	Intensity (a.u.)	Mass accuracy (ppm)
PI(34:1)	$[C_{43}H_{80}O_{13}P]^-$	835.5342	$8.35x10^4$	-1.3
PI(36:4)	$[C_{45}H_{78}O_{13}P]^-$	857.5186	$1.20x10^5$	0.3
PI(38:3)	$[C_{47}H_{80}O_{13}P]^-$	883.5342	$9.73x10^4$	0.4
PI(38:4)	$[C_{47}H_{82}O_{13}P]^-$	885.5499	$8.99x10^6$	0.6
PA(32:0)	$[C_{35}H_{68}O_8P]^-$	647.4657	$1.08\ x10^4$	1.3
PA(34:1)	$[C_{37}H_{70}O_8P]^-$	673.4814	$2.13\ x10^5$	0.8
PA(36:1)	$[C_{39}H_{72}O_8P]^-$	699.4970	$2.06\ x10^5$	0.9
PA(36:2)	$[C_{39}H_{74}O_8P]^-$	701.5127	$4.28\ x10^6$	0.9
PA(38:1)	$[C_{41}H_{78}O_8P]^-$	729.5440	$4.60\ x10^4$	1.1
PA(38:2)	$[C_{41}H_{76}O_8P]^-$	727.5283	$4.05\ x10^4$	0.9
PA(38:3)	$[C_{41}H_{74}O_8P]^-$	725.5127	$1.00\ x10^4$	1.6
PA(38:4)	$[C_{41}H_{72}O_8P]^-$	723.4970	$7.25\ x10^4$	0.8
PA(38:5)	$[C_{41}H_{70}O_8P]^-$	721.4814	$1.10\ x10^4$	0.9
PA(40:1)	$[C_{43}H_{82}O_8P]^-$	757.5753	$9.10\ x10^3$	0.6
PA(40:2)	$[C_{43}H_{80}O_8P]^-$	755.5596	$1.35\ x10^4$	0.4
PA(40:4)	$[C_{43}H_{76}O_8P]^-$	751.5283	$5.08\ x10^4$	0.7
PA(40:5)	$[C_{43}H_{74}O_8P]^-$	749.5127	$9.78\ x10^3$	1.0
PA(40:6)	$[C_{43}H_{72}O_8P]^-$	747.4970	$1.47\ x10^6$	0.8
PS(36:1)	$[C_{42}H_{79}NO_{10}P]^-$	788.5447	$5.43x10^5$	0.5
PS(36:2)	$[C_{42}H_{77}NO_{10}P]^-$	786.5291	$1.12x10^4$	0.4
PS(38:4)	$[C_{44}H_{77}NO_{10}P]^-$	810.5291	$5.68x10^4$	-1.6
PS(40:6)	$[C_{46}H_{77}NO_{10}P]^-$	834.5291	$1.97x10^5$	0.3
PE(34:0)	$[C_{39}H_{77}NO_8P]^-$	718.5392	$4.76\ x10^4$	0.9
PE(34:1)	$[C_{39}H_{75}NO_8P]^-$	716.5236	$2.68\ x10^4$	1.0
PE(36:1)	$[C_{41}H_{79}NO_8P]^-$	744.5549	$3.74\ x10^5$	0.8
PE(36:2)	$[C_{41}H_{77}NO_8P]^-$	742.5392	$3.00\ x10^4$	0.9
PE(36:4)	$[C_{41}H_{73}NO_8P]^-$	738.5079	$1.11\ x10^4$	0.6
PE(38:1)	$[C_{43}H_{83}NO_8P]^-$	772.5862	$2.31\ x10^4$	0.5
PE(38:2)	$[C_{43}H_{81}NO_8P]^-$	770.5705	$9.48\ x10^3$	0.6
PE(38:4)	$[C_{43}H_{77}NO_8P]^-$	766.5392	$4.48\ x10^5$	0.6
PE(38:5)	$[C_{43}H_{75}NO_8P]^-$	764.5236	$1.11\ x10^4$	0.6
PE(38:6)	$[C_{43}H_{73}NO_8P]^-$	762.5079	$2.68\ x10^4$	0.2
PE(40:4)	$[C_{45}H_{81}NO_8P]^-$	794.5705	$2.12x10^4$	0.3
PE(40:6)	$[C_{45}H_{77}NO_8P]^-$	790.5392	$4.28x10^5$	0.5

Nature Methods: doi:10.1038/nmeth.4504

PE(O-34:2) or PE(P-34:1)	$[C_{39}H_{75}NO_7P]^-$	700.5287	1.46×10^5	0.9
PE(O-36:1) or PE(P-36:0)	$[C_{41}H_{77}NO_7P]^-$	726.5443	9.19×10^5	0.9
PE(O-36:2) or PE(P-36:1)	$[C_{41}H_{79}NO_7P]^-$	728.5600	5.80×10^5	0.9
PE(O-38:2) or PE(P-38:1)	$[C_{43}H_{83}NO_7P]^-$	756.5913	8.67×10^4	0.5
PE(O-38:3) or PE(P-38:2)	$[C_{43}H_{81}NO_7P]^-$	754.5756	2.84×10^5	0.5
PE(O-38:5) or PE(P-38:4)	$[C_{43}H_{77}NO_7P]^-$	750.5443	1.01×10^5	0.5
PE(O-38:6) or PE(P-38:5)	$[C_{43}H_{75}NO_7P]^-$	748.5287	3.94×10^4	0.7
PE(O-40:3) or PE(P-40:4)	$[C_{45}H_{81}NO_7P]^-$	778.5756	6.70×10^4	0.5
PE(O-40:4) or PE(P-40:5)	$[C_{45}H_{79}NO_7P]^-$	776.5600	1.24×10^5	0.6
PE(O-40:5) or PE(P-40:6)	$[C_{45}H_{77}NO_7P]^-$	774.5443	2.09×10^5	0.5
PE(O-40:6) or PE(P-40:7)	$[C_{45}H_{75}NO_7P]^-$	772.5287	2.26×10^4	0.3

Supplementary Table 4. Putative annotation of sterol species detected in the negative ion image of the mouse hippocampus in Figure 3D (main text).

Lipid	**Chemical formula of $[M-H]^-$ ion**	**Mass (Da)**	**Intensity (a.u.)**	**Mass accuracy (ppm)**
Sterols				
CH	$[C_{27}H_{45}O]^-$	385.3476	5.51×10^6	0.8
CH sulfatide	$[C_{27}H_{45}O_4S]^-$	465.3044	7.93×10^6	0.6
zymosterone	$[C_{27}H_{41}O]^-$	381.3222	7.51×10^5	0.8
desmosterol	$[C_{27}H_{43}O]^-$	383.3319	1.30×10^7	0.8

Supplementary Table 5. Putative annotation of Fatty Acid (FA) species detected in the negative ion image of the mouse hippocampus in Figure 3D (main text).

Lipid	**Chemical formula of $[M-H]^-$ ion**	**Mass (Da)**	**Intensity (a.u.)**	**Mass accuracy (ppm)**
Fatty Acids Note: To a large extent FA signals are assumed to be caused by fragmentation from larger acyl lipids, rather than being free FA.				
FA(12:0)	$[C_{12}H_{23}O_2]^-$	199.1704	6.78×10^4	0.3
FA(14:0)	$[C_{14}H_{27}O_2]^-$	227.2017	4.15×10^5	1.0
FA(16:0)	$[C_{16}H_{31}O_2]^-$	255.2330	4.53×10^8	0.8
FA(16:1)	$[C_{16}H_{29}O_2]^-$	253.2173	1.78×10^7	0.8
FA(16:2)	$[C_{16}H_{27}O_2]^-$	251.2017	1.10×10^5	0.7
FA(18:0)	$[C_{18}H_{35}O_2]^-$	283.2643	8.12×10^8	0.5
FA(18:1)	$[C_{18}H_{33}O_2]^-$	281.2486	7.62×10^8	0.4
FA(18:2)	$[C_{18}H_{31}O_2]^-$	279.2330	3.95×10^7	0.4
FA(18:3)	$[C_{18}H_{29}O_2]^-$	277.2173	6.09×10^4	0.3
FA(18:4)	$[C_{18}H_{27}O_2]^-$	275.2017	8.05×10^3	0.4
FA(20:0)	$[C_{20}H_{39}O_2]^-$	311.2956	4.56×10^6	0.7

Nature Methods: doi:10.1038/nmeth.4504

FA(20:1)	$[C_{20}H_{37}O_2]^-$	309.2799	1.06×10^8	0.6
FA(20:2)	$[C_{20}H_{35}O_2]^-$	307.2643	6.62×10^6	0.6
FA(20:3)	$[C_{20}H_{33}O_2]^-$	305.2486	9.47×10^6	0.5
FA(20:4)	$[C_{20}H_{31}O_2]^-$	303.2330	1.60×10^8	0.4
FA(22:0)	$[C_{22}H_{43}O_2]^-$	339.3269	1.35×10^6	0.3
FA(22:1)	$[C_{22}H_{41}O_2]^-$	337.3112	1.15×10^7	0.7
FA(22:2)	$[C_{22}H_{39}O_2]^-$	335.2956	3.62×10^5	0.7
FA(22:3)	$[C_{22}H_{37}O_2]^-$	333.2799	9.77×10^5	0.7
FA(22:4)	$[C_{22}H_{35}O_2]^-$	331.2643	6.18×10^7	0.6
FA(22:5)	$[C_{22}H_{33}O_2]^-$	329.2486	1.66×10^6	0.6
FA(22:6) DHA	$[C_{22}H_{31}O_2]^-$	327.2330	4.84×10^7	0.5
FA(24:0)	$[C_{24}H_{45}O_2]^-$	365.3425	3.06×10^6	0.4
FA(24:0)	$[C_{24}H_{47}O_2]^-$	367.3582	8.69×10^5	0.5
FA(24:2)	$[C_{24}H_{43}O_2]^-$	363.3269	8.26×10^4	0.9
FA(24:3)	$[C_{24}H_{41}O_2]$	361.3112	1.44×10^4	1.0
FA(24:4)	$[C_{24}H_{39}O_2]^-$	359.2956	2.30×10^5	0.8
FA(24:5)	$[C_{24}H_{37}O_2]^-$	357.2799	2.29×10^4	0.8
FA(24:6)	$[C_{24}H_{35}O_2]^-$	355.2643	1.30×10^4	1.0
FA(26:0)	$[C_{26}H_{51}O_2]^-$	395.3895	1.39×10^4	0.4
FA(26:1)	$[C_{26}H_{49}O_2]^-$	393.3738	2.59×10^4	0.9
FA(26:2)	$[C_{26}H_{47}O_2]^-$	391.3582	9.11×10^3	1.5
FA(26:3)	$[C_{26}H_{45}O_2]^-$	389.3425	8.10×10^3	1.8
FA(26:4)	$[C_{26}H_{43}O_2]^-$	387.3269	9.52×10^3	0.9
FA(26:5)	$[C_{26}H_{41}O_2]^-$	385.3112	7.45×10^3	0.9
FA(26:6)	$[C_{26}H_{39}O_2]^-$	383.2956	7.20×10^3	0.4
FA(28:5)	$[C_{28}H_{45}O_2]^-$	413.3425	8.99×10^3	0.7
FA(28:6)	$[C_{28}H_{43}O_2]^-$	411.3269	9.72×10^3	1.2

Supplementary Table 6. Putative annotation of small biomolecules and metabolite species detected in the negative ion image of the mouse hippocampus in Figure 3D (main text).

Lipid	**Chemical formula of $[M-H]^-$ ion**	**Mass (Da)**	**Intensity (a.u.)**	**Mass accuracy (ppm)**
Small biomolecules /Metabolites				
Pyruvic acid	$[C_3H_3O_3]^-$	87.0088	2.00×10^7	-3.0
Lactic acid	$[C_3H_5O_3]^-$	89.0244	1.84×10^5	-2.6
GABA	$[C_4H_8NO_2]^-$	102.0561	3.19×10^6	-0.6
Serine	$[C_3H_6NO_3]^-$	104.0353	1.18×10^4	0.2
Cytosine	$[C_4H_4N_3O]^-$	110.0360	9.15×10^4	0.8
Uracil	$[C_4H_3N_2O_2]^-$	111.0200	5.80×10^6	0.8
Proline	$[C_5H_8NO_2]^-$	114.0561	4.20×10^4	0.5
Valine	$[C_5H_{10}NO_2]^-$	116.0717	1.12×10^4	1.0
Methylcytosine	$[C_5H_6N_3O]^-$	124.0516	7.96×10^4	0.4
Thymine	$[C_5H_5N_2O_2]^-$	125.0357	4.23×10^6	0.4
Isoleucine/leucine	$[C_6H_{12}NO_2]^-$	130.0874	2.87×10^4	0.3

Nature Methods: doi:10.1038/nmeth.4504

Asparagine	$[C_4H_7N_2O_3]^-$	131.0462	9.29×10^3	-0.3
Adenine	$[C_5H_4N_5]^-$	134.0472	3.53×10^7	1.1
Hypoxanthine	$[C_5H_3N_4O]^-$	135.0312	7.42×10^6	0.8
Glutamine	$[C_5H_9N_2O_3]^-$	145.0619	4.56×10^4	0.6
Lysine	$[C_6H_{13}N_2O_2]^-$	145.0983	2.07×10^4	0.7
Glutamic acid	$[C_5H_8NO_4]^-$	146.0459	9.31×10^4	0.6
Guanine	$[C_5H_4N_5O]^-$	150.0421	6.02×10^5	0.2
Dopamine	$[C_8H_{10}NO_2]^-$	152.0717	1.69×10^5	0.4
Glycerol-3-phosphate	$[C_3H_6O_5P]^-$	152.9961	6.10×10^7	0.4
Histidine	$[C_6H_8N_3O_2]^-$	154.0622	1.00×10^5	0.6
Aspartic acid	$[C_6H_6NO_4]^-$	156.0302	1.00×10^4	0.8
Phenylalanine	$[C_9H_{10}NO_2]^-$	164.0717	5.61×10^4	0.1
Phosphocholine-CH3	$[C_4H_{11}NO_4P]^-$	168.0431	1.37×10^5	0.3
Tyrosine	$[C_9H_{10}NO_3]^-$	180.0666	1.63×10^4	0.9
Tryptophan	$[C_{11}H_{11}N_2O_2]^-$	203.0826	3.07×10^4	0.6
Inosine	$[C_{10}H_{11}N_4O_5]^-$	267.0735	5.96×10^4	0.6
cAMP	$[C_{10}H_{11}N5O_6P]^-$	328.0452	1.10×10^4	-1.2
AMP	$[C_{10}H_{13}N5O_7P]^-$	346.0558	9.69×10^4	0.5
GMP	$[C_{10}H_{13}N_5O_8P]^-$	362.0507	4.58×10^3	2.3
C16 taurine	$[C_{18}H_{36}NO_4S]^-$	362.2371	4.83×10^5	0.9
C18:1 taurine	$[C_{20}H_{38}NO_4S]^-$	388.2527	2.50×10^5	0.9
C18 taurine	$[C_{20}H_{40}NO_4S]^-$	390.2684	2.20×10^5	0.9

Supplementary Table 7. Putative annotation of positive ion glycerophospholipid biomolecules and metabolite species detected from the CA3 vicinity of the hippocampus on a coronal brain section.

Lipid	**Ion species**	**Chemical Formula**	**Mass (Da)**	**Intensity (a.u.)**	**Mass accuracy (ppm)**
Glycerophosphocholines					
PC(36:1)	$[M+K]^+$	$C_{44}H_{86}NO_8PK$	826.5728	2.48×10^5	1.5
	$[M+Na]^+$	$C_{44}H_{86}NO_8PNa$	810.5989	1.34×10^4	1.1
	$[M+K\text{-}N(CH_3)_3]^+$	$C_{41}H_{77}O_8PK$	767.4993	1.55×10^5	1.7
PC(36:2)	$[M+K]^+$	$C_{44}H_{84}NO_8PK$	824.5572	1.04×10^4	1.3
PC(34:0)	$[M+K]^+$	$C_{42}H_{84}NO_8PK$	800.5572	4.56×10^4	1.3
	$[M+K\text{-}N(CH_3)_3]^+$	$C_{39}H_{75}O_8PK$	741.4837	3.10×10^4	1.6
PC(34:1)	$[M+K]^+$	$C_{42}H_{82}NO_8PK$	798.5415	2.47×10^6	1.6
	$[M+Na]^+$	$C_{42}H_{82}NO_8PNa$	782.5676	1.43×10^5	1.6
	$[M+H]^+$	$C_{42}H_{83}NO_8P$	760.5856	4.89×10^4	1.8
	$[M+K\text{-}N(CH_3)_3]^+$	$C_{39}H_{73}O_8PK$	739.4680	1.82×10^6	0.6

Nature Methods: doi:10.1038/nmeth.4504

	$[M+Na-N(CH_3)_3]^+$	$C_{39}H_{73}O_8PNa$	723.4941	3.81×10^4	1.8
PC(33:0)	$[M+K]^+$	$C_{40}H_{78}NO_8PK$	770.5102	9.34×10^3	0.9
PC(32:0)	$[M+K]^+$	$C_{40}H_{80}NO_8PK$	772.5259	1.50×10^6	1.6
	$[M+Na]^+$	$C_{40}H_{80}NO_8PNa$	756.5519	5.76×10^4	1.9
	$[M+H]^+$	$C_{40}H_{81}NO_8P$	734.5700	1.75×10^4	1.6
	$[M+K- N(CH_3)_3]^+$	$C_{37}H_{71}O_8PK$	713.4524	9.67×10^5	1.8
	$[M+Na-N(CH_3)_3]^+$	$C_{37}H_{71}O_8PNa$	697.4784	1.64×10^4	1.9

Supplementary Table 8. Putative annotation of sphingolipids detected in the brain tissue in positive ion mode.

Lipid	Ion species	Chemical Formula	Mass (Da)	Intensity (a.u.)	Mass accuracy (ppm)
Sphingolipids					
GlcCer(42:2)	$[M+K+H_20]^+$	$C_{48}H_{93}NO_9K$	866.6487	3.79×10^4	1.4
	$[M+K]^+$	$C_{48}H_{91}NO_8K$	848.6382	2.79×10^4	1.4
	$[M+Na]^+$	$C_{48}H_{91}NO_8Na$	832.6642	1.57×10^4	1.5
GlcCer(42:3)	$[M+K+ H_20]^+$	$C_{48}H_{91}NO_9K$	864.6331	2.04×10^4	1.5
GlcCer(40:2)	$[M+K+ H_20]^+$	$C_{46}H_{89}NO_9K$	838.6174	5.53×10^4	1.5
SM(d18:1/18:0)	$[M+K]^+$	$C_{41}H_{83}N_2O_6PK$	769.5626	7.22×10^4	1.7
SM(d18:1/18:0)	$[M+K- N(CH_3)_3]^+$	$C_{41}H_{83}N_2O_6PK$	710.4891	8.07×10^4	1.8

Supplementary Table 9. Putative annotation of glycerophosphocholines species detected in the macrophages

Lipid	Ion species	Chemical Formula	Mass Da	Cell condition (treated / control)
Glycerophosphocholines				
PC(36:1)	$[M+K]^+$	$C_{44}H_{86}NO_8PK$	826.5728	control
	$[M+Na]^+$	$C_{44}H_{86}NO_8PNa$	810.5989	treated
	$[M+K-N(CH_3)_3]^+$	$C_{41}H_{77}O_8PK$	767.4993	control
PC(36:2)	$[M+K]^+$	$C_{44}H_{84}NO_8PK$	824.5572	treated
PC(34:1)	$[M+K]^+$	$C_{42}H_{82}NO_8PK$	798.5415	control

Nature Methods: doi:10.1038/nmeth.4504

	$[M+Na]^+$	$C_{42}H_{82}NO_8PNa$	782.5676	treated
	$[M+H]^+$	$C_{42}H_{83}NO_8P$	760.5856	treated
	$[M+K-N(CH_3)_3]^+$	$C_{39}H_{73}O_8PK$	739.4680	control
PC(32:0)	$[M+K]^+$	$C_{40}H_{80}NO_8PK$	772.5259	treated
	$[M+H]^+$	$C_{40}H_{81}NO_8P$	734.5700	treated

Nature Methods: doi:10.1038/nmeth.4504